

Tetradentate iminophenolate copper complexes in *rac*-lactide polymerization

*Pargol Daneshmand, Aurélie Randimbiarisololo, Frank Schaper**

Centre in Green Chemistry and Catalysis, Département de chimie, Université de Montréal, 2900
Boul. E.-Montpetit, Montréal, QC, H3T 1J4, Canada

* Frank.Schaper@umontreal.ca

Draft

Abstract

Copper(II) nitrate complexes of 2-(((2-((2-aminoethyl)amino)ethyl)imino)methyl)phenol, 2-(((2-((2-aminoethyl)amino)ethyl)imino)methyl)-4,6-dichlorophenol, 2-(((2-(piperazin-1-yl)ethyl)imino)methyl)phenol and (2,4-di-tert-butyl-6-(((2-(piperazin-1-yl)ethyl)imino)methyl)phenol, as well as a copper(II) acetate complex of 2-(((2-(piperidin-1-yl)ethyl)imino)methyl)phenol have been prepared and characterized by X-ray diffraction studies. In combination with benzyl alcohol, all complexes are active in *rac*-lactide polymerization at 140 °C in molten monomer to provide moderately heterotactic PLA. Most complexes showed complicated reaction kinetics, indicative of two interconverting active species. Molecular weight control was poor and a strong tendency toward intramolecular transesterification led to oligomeric products. There was no indication that the basic site of the ligand is participating in the polymerization reaction by deprotonation of the alcohol nucleophile.

Keywords

Copper complexes – Catalysis – Polymerization – *rac*-Lactide

Introduction

Poly(lactic acid) (PLA), produced from ring-opening polymerization of lactide, is one of the most important biopolymers today.¹⁻⁷ Controlled polymerization of lactide has become a catalytic challenge,⁷⁻³³ but combining isotactic stereocontrol, polymer molecular weight control with high activity and catalyst stability remains difficult to achieve. Most studies – including our own – focus on coordination-insertion polymerization of lactide, since the tight four-membered metallacycle of the insertion transition state is likely to be highly influenced by the ligand environment, which in turn would allow control over relative reactivities (Scheme 1). A major drawback of lactide polymerization by a coordination-insertion mechanism is the inherent lability of the metal alkoxide catalyst towards protonation. Most coordination-insertion polymerization catalysts thus do not or would not survive conditions currently employed in the industrial production of PLA, i. e. the presence of notable amounts of water and lactic acid at temperatures of 140 °C and above. An alternative pathway to ring-opening polymerization of lactide is Lewis-acid activation of the monomer (Scheme 1).³⁴⁻³⁶ Since metal alkoxides are not required, the mechanism typically tolerates protic substances, as long as the spectator ligand is not protonated easily. Polymerizations by an activated-monomer mechanism are, however, more difficult to control, since the nucleophilic attack occurs at some distance from the metal center and since the activated-monomer complex is highly flexible. Lewis-acid-catalyzed lactide polymerizations thus typically show only low to moderate stereocontrol, typically to heterotactic PLA and mainly due to the interaction of the chiral polymeryl alcohol with the monomer without much influence from the catalytic site. In 2013, Sarazin and Carpentier explained an increased activity in rare-earth-based catalysts with a “*ligand-assisted activated monomer mechanism*”.³⁷ A basic site at the ligand can interact with the alcohol

nucleophile by hydrogen bonding, thus facilitating the nucleophilic attack on the monomer (Scheme 1). This parallels work by Bourissou and Maron on sulfonic acid-catalyzed caprolactone polymerization, where they showed that sulfonic acid acts as Brønsted acid and base at the same time.³⁸ In contrast to ordinary activation of the monomer, interaction with the catalytic site now requires a well-defined and relatively rigid geometry. In a series of excellent publications, Wu and coworkers employed this concept in lactide polymerizations with phenolate complexes of group 1 metals, mostly sodium and potassium.^{36, 39-44} They could show that phenolate is not incorporated in the polymer chain and acts (mostly) as spectator ligand. The bulky environment (crown-ether coordination around the metal center, highly substituted phenolates) constricts the environment sufficiently to allow stereocontrol, remarkably toward isotactic PLA. The catalysts are itself achiral (although chirality at the metal is possible in the transition state) and the stereocontrol mechanism was found to be chain-end control.

In the following we explore the possibility to apply this stereocontrol mechanism to copper(II) complexes. Iminophenolate Schiff-base ligands provide highly stable six-membered metallacycles and are one of the most common motifs in coordination chemistry. Iminophenolate complexes were among the first complexes employed in lactide polymerization.⁴⁵⁻⁴⁸ In copper based lactide polymerization, typically homoleptic diphenolate complexes or salen ligands, which can be considered their cyclic analogs, have been employed (Scheme 2).⁴⁹⁻⁵³ Here we investigate heteroleptic complexes of tetradentate ligand **L1** with a weakly coordinating anion (**A**, Scheme 2). Formation of a cationic complex should increase activity in an activated-monomer mechanism and the dissociation of the terminal amino ligand upon coordination of the monomer (claimed, for example, in similar tridentate zinc complexes)⁵⁴⁻⁵⁵ will liberate a basic site available for interaction with the alcohol

nucleophile. It should be noted that zinc complexes with similar tetradentate linear triaminophenolate ligands have been recently employed by Kol for isotactic lactide polymerization.⁵⁶ These complexes followed a coordination-insertion mechanism, however, different from the mechanism targeted here.

Results and discussions

Copper complexes of type **A** have been reported for a variety of anions. Structurally characterized (**L1**)CuX complexes have been reported for $X^- = PF_6^-, ClO_4^-, Br^-,$ and Cl^- .⁵⁷⁻⁶² We were most interested in the respective nitrate complex, (**L1**)Cu(NO₃), **1**, which was prepared by reaction of copper nitrate with **L1H** in methanol (Scheme 3). Complex **1** crystallizes as a monomeric, cationic complex with square-pyramidal geometry. A water molecule replaced the anion and occupies the apical position (Fig. 1, Table 1). The respective triflate complex **2** was prepared analogously and is practically isostructural (Scheme 3, Fig. 1, Table 1). Reaction with chloro-substituted ligand **L2H** provided **3**. In **3**, the nitrate anion instead of water is coordinated to Cu and bridges two copper centers to form a 1D coordination polymer. Crystal quality was bad for **3** and the structure should not be considered more than proof of connectivity.

Complexes **1** and **2** were tested for the polymerization of *rac*-lactide at 140 °C in molten monomer with benzyl alcohol as a co-initiator. **1** showed only low to moderate activity, requiring 24 h to complete conversion. Conversion-time plots of an experiment in which the pressure tube was opened and aliquots taken (Fig. 2, squares; Tables 2 and S1, entry 7) and the results of separate experiments quenched at a given time (Fig. 2, diamonds; Table S1, entries 1-6) show very similar conversions. Introduction of ambient atmosphere during sampling thus does not seem to influence the reaction. To test this, polymerizations were

conducted in the presence of 5 equiv acetic acid or 5 equiv water (Tables 2 and S1, entries 11 and 12). Activity was unaffected by acetic acid and even increased upon addition of water (Fig. S1). Polymer molecular weight analysis would normally provide evidence whether water was just tolerated or act as a chain-transfer reagent. However, polymer molecular weights for **1** were much lower than expected (Tables 2 and S1). MALDI-MS spectra confirmed the presence of cyclic oligomers (Fig. S12), indicative of intramolecular transesterification, and polymer molecular weights could thus not be used for mechanistic interpretations. The same tendency for intramolecular transesterification was observed for all other catalysts in this study, which generally produced oligomers instead of polymers (Tables 2 and S1, Fig. S12-S15). Polymerizations in the presence of ligand **L1H** instead of the respective copper complex resulted in only 11% conversion over 24 h with BnOH as initiator (Table S1).

Activities in polymerizations following an activated monomer-mechanism typically increase with increasing concentration of the alcohol nucleophile. Addition of 2, 4, or 8 equiv of benzyl alcohol indeed led to the expected increase in reactivity, but the increase was not linear and showed saturation behaviour (Fig. 3, Table S1, entries 8-10). While we did not investigate this in detail, it is possible that the alcohol pre-coordinates either to the copper center or via hydrogen-bonding with basic sites at the ligand. Saturation of the pre-coordination equilibrium would account for the observed Michaelis-Menten kinetics. While all kinetic traces could be fitted to a first-order rate law for conversions <70%, conversions at later stages of the reaction were higher than expected, which will be discussed later.⁶³

Triflate complex **2** likewise polymerized lactide with essentially identical activity, but showed a pronounced induction period (Fig. 4, Tables 2 and S1, entry 17). To further test the influence of the anion, polymerizations with **1** were conducted in the presence of 1 or 4

equiv of $[\text{NEt}_4]\text{Cl}$ or $[\text{NEt}_3\text{H}][\text{TsO}]$ ($[\text{TsO}]^- = \text{tosylate}$, Fig. 5, Tables 2 and S1, entries 13-16). The presence of a more coordinating anion resulted in an observable induction period (conversions are below those of **1** without added salt for $t < 60$ min), but final activities were 3 times higher than without addition of salt ($k_{\text{obs}} = 0.4 \text{ h}^{-1}$). Given that $[\text{NEt}_4]\text{Cl}$ and $[\text{NEt}_3\text{H}][\text{TsO}]$, either at 1 or 4-fold concentration relative to **1**, yield virtually identical kinetic traces, the observed increase in activity is most likely due to a rate increase of **1** under those conditions. In combination with the positive deviation of conversion from the theoretical curves observed above and the higher activity in presence of water, this indicates that **1** slowly converts into a more active state and that this conversion is more efficient under more polar conditions.

Kinetics of polymerizations with **3**, with a dichloro-substituted phenolate ligand, supported this interpretation. Conversion-time plots of **3** in the presence of either 1 or 4 equivalents of benzyl alcohol are close to linear (Fig. 6, Tables 2 and S1, entries 18+19). There is no mechanistic explication for a zero-order dependence on lactide concentration, in particular since the immediate and consistent colour change of the reaction mixture indicates that **3** dissolves readily in lactide monomer. The semilogarithmic plot for both reactions does not show the gradual increase to a linear regime expected for first-order reactions with an induction period either, but rather two linear regimes with different rate constants (Fig. 6). **1** and **3** thus slowly convert from a state of lower reactivity (active immediately or with very short induction periods) to a state of higher reactivity throughout the reaction, which occurs at an earlier stage for **3**.

Polymerizations with **1-3** all afforded moderately heterotactic PLA ($P_T = 0.7-0.85$, Table 2). Heterotacticities differed notably between different experiments under otherwise similar conditions, but there was no clear correlation between stereocontrol and either the catalyst

employed, addition of benzyl alcohol or ammonium salts (Table S1). To investigate in more detail the influence of a basic group on the ligand on catalyst reactivity, the ethylene diamine moiety was replaced by piperazine (**L3H**, Scheme 4). Although sterically similar, coordination of both amino groups in piperazine would enforce an unfavourable boat-conformation, and consequently in structurally characterized copper complexes with **L3** or ligands similar to **L3** the ligand was tridentate.⁶⁴⁻⁷⁴ Complexes **4** and **5** were prepared analogous to **1**. In addition, **6** was prepared, which is sterically similar but does not contain a basic group on the ligand. Reaction with copper(II) nitrate did not afford crystalline material upon reaction with **L4H** (even in the presence of base), but **6** was readily obtained with an acetate counteranion (Scheme 4). Complexes **4** and **5** also crystallized as monomeric complexes with square-pyramidal coordination geometry. A derivative structure of **4** with nitrate replaced by a water ligand has been reported previously.⁶⁸ **6** forms a 1D coordination polymer by bridging coordination of the acetate anion, similar to the structure of **3**. In all three complexes, there is a weak interaction with a second oxygen on the nitrate or acetate anion. **4** and **5** were obtained as the nitric acid adducts with an additional anion and a protonated terminal amino group on the piperazine. This is in accordance with all other structurally characterized copper complexes of ligands of type **L5**.⁶⁴⁻⁷⁴ Several attempts to prepare the nitric-acid-free complex by introducing bases in the reaction failed to provide crystalline material. The anion is coordinated in all three complexes in an equatorial position. The apical position is either occupied by a second anion or methanol, with the elongation of the bond length expected for the ligand in the apical position (Table 1).

The kinetic profile of *rac*-lactide polymerizations with **4** showed again an apparent linear conversion-time plot, which deviates significantly from the sigmoidal curve expected for a

simple induction period. Conversions from four independent kinetic experiments and from four separate experiments quenched at a given polymerization time agree remarkably well with each other (Fig. 8, Tables 2 and S1, entries 21-30), indicating again that sample-taking did not influence polymerization and that the observed deviations from simple first-order behaviour are reproducible. The semilogarithmic plot shows again two linear regimes, in agreement with slow transformation from one active species into another (Fig. 8). Activities somewhat increase with addition of benzyl alcohol (Fig. S2-S4, Table S1, entries 20,31-33), but the saturation behaviour is even more pronounced than in **1**. Polymerizations at lower and increased catalyst loading yield reduced or increased rate constants for the slow regime at the beginning of the reaction as well as for the fast regime at the end of the reaction (Fig. S5-S7, Tables 2 and S1, entries 34+35). Given the two regimes present, the quality of the data is insufficient to determine the actual reaction order in catalyst with confidence, but the obtained data agrees reasonably well with a linear dependence on catalyst concentration with a “dead” concentration of 0.3 mol% catalyst (Fig. S7). At 4:lactide = 1:50, the reaction follows pure first-order kinetics (Fig. S5, S6), eventual for the trivial reason that the reaction already reached 90% conversion at the time the second active species typically starts to be noticeable in the reaction kinetics.

Polymerizations with **4** showed the same moderate heterotacticity as **1-3** with $P_r = 0.7-0.8$. Polymerizations were conducted in the presence of base (1 equiv of triethylamine, pyridine, or *t*BuOK per **4**) to ensure that the ammonium group on piperazine is available for interaction with the alcohol (Fig. S8+S9, Table S1, entries 36-38). An induction period was observed for triethylamine and pyridine, to lead afterwards to faster conversion than without added base. Polymerizations showed slightly higher stereocontrol in the presence of pyridine and triethylamine ($P_r = 0.73-0.87$, Table 2, S1), but lower stereocontrol for *t*BuOK

($P_r = 0.5-0.7$), which would be suspected to be most effective in deprotonating the ammonium group. The slightly increased stereocontrol can thus not be correlated with liberation of a basic site on the ligand.

Introduction of *tert*-butyl substituents at the *ortho* and *para*-position of the phenolate ligand in **5** leads to a minor reduction in activity (approx. 2/3 compared to **4**), but otherwise identical polymerization behaviour (Fig. S10 and S11, Tables 2 and S1, entries 39-41). Stereocontrol was only slightly increased with the more bulky phenolate ligand ($P_r = 0.75-0.85$). Polymerizations with **6**, carrying a tridentate ligand without additional basic site, show the same general polymerization behaviour as **1-5** (Fig. 9, Tables 2 and S1, entries 42-44). Coordination/dissociation of the 3rd amino group is thus not responsible for the existence of two active species. Rate constants identical in the range of error to those of **4** and unaffected stereocontrol of $P_r = 0.75-0.80$ further support that the 3rd amino group in **4** does not participate in the polymerization.

Conclusions

While the structure of the active species is not known, close to identical activities and polymerization kinetics of complexes with diethylenetriamine, piperazineethyleneamine and piperidineethyleneamine substituents propose a tridentate coordination of the ligand in the active species. However, there is no evidence that a basic site facilitates polymerization via a *ligand-assisted chain-end control* mechanism in these complexes.

Complexes **1-6** show up to 85% heterotacticity, an impressive stereocontrol for polymerizations at 140 °C and unprecedented for copper complexes. The high amount of intramolecular transesterification observed for all complexes, however, and the at best

mediocre activity argues against the suitability of this catalyst system for lactide polymerization in general. Given the fact that copper diketiminate complexes with a *bidentate* ligand, square-planar geometry and notable steric bulk oriented below and above the complex plane did not show any evidence of transesterification reactions even under monomer-starved conditions,⁷⁵⁻⁷⁶ it can be argued that ligands which permit square-pyramidal coordination might not provide a constricted enough coordination environment to avoid transesterification reactions.

Experimental section

General. 4,6-di-*tert*-Butylsalicylaldehyde,⁷⁷ 1,3-dichlorosalicylaldehyde,⁷⁷ **L1H**,⁶⁰ **L3H**,⁷² **L4H**,⁷⁸ and **L5H**,⁷⁹ were prepared according to literature. *rac*-Lactide (98%) was purchased from Sigma–Aldrich, purified by 3x recrystallization from dry ethyl acetate and kept at $-30\text{ }^{\circ}\text{C}$. All other chemicals were purchased from common commercial suppliers and used without further purification. ^1H and ^{13}C NMR spectra were acquired on Bruker Avance 300 and 400 spectrometers. Chemical shifts were referenced to the residual signals of the deuterated solvents (CDCl_3 : ^1H : δ 7.26 ppm, ^{13}C : δ 77.16). Proton and carbon signals of minor isomers are respectively reported in brackets. Abbreviations for peak multiplicities are s (singlet), d (doublet), t (triplet), q (quadruplet), qu (quintuplet), m (multiplet) and br (broad). Certain ^{13}C NMR chemical shifts values were extracted from HSQC and HMBC spectra. Elemental analyses were performed by the Laboratoire d'analyse élémentaire (Université de Montréal). All UV-Vis measurements were done in MeOH at RT in a sealed quartz cell on a Cary 500i UV-Vis-NIR Spectrophotometer.

2-(2-(2-aminoethylamino)ethylimino)methyl)-4,6-dichlorophenol, L2H. A procedure from literature was adapted as follows:⁷⁸ To a yellow solution of 1,3-dichlorosalicylaldehyde (1.00 g, 5.2 mmol) in ethanol (10 mL) was added dropwise a solution of diethylenetriamine (540 mg, 5.2 mol) in ethanol (10 mL), followed by the addition of 5 drops of formic acid. The obtained yellow solution was refluxed for 1 hour. The solvent was removed under vacuum to yield a yellow oil (1.26 g, 87%).

^1H NMR (CDCl_3 , 300 MHz): δ 8.22 (br s, 1H, H³), 7.37 (dd, J = 3, 3 Hz, 1H, H¹), 7.12 (d, J = 3 Hz, 0.6H, H²), [7.08 (d, J = 3 Hz, 0.4H, H²)], 3.67 (br s, 2H, H⁴), 2.97 (br s, 2H, H⁵), 2.80 (t, J = 6 Hz, 2H, H⁷), 2.68 (t, J = 6 Hz, 2H, H⁶); $^{13}\text{C}\{^1\text{H}\}$ NMR (CDCl_3 , 75 MHz): δ 164.5 (HSQC, CH³), [158.3 (HMBC, C-OH)], 157.8 (HMBC, C-OH) [132.6 (CH¹)], 132.2 (CH¹), [129.1, CH²], 129.0 (CH²), 123.3 (CC¹),

122.4 (2C, CCl² + C(C=N)), 58.1 (CH⁴), 52.4 (CH⁶), 49.8 (CH⁵), 41.9 (CH⁷), [41.6 (CH⁷)]. ESI-HRMS (m/z): [M+H]⁺ (C₁₁H₁₆Cl₂N₃O) calcd 276.0670; found 276.0675.

[(L1)Cu][NO₃]₂·H₂O, 1. Cu(NO₃)₂·2.5 H₂O (112 mg, 0.48 mmol) was added to a freshly prepared yellow solution of 2-(2-(2-aminoethylamino)ethylimino)methylphenol (**L1H**) (100 mg, 0.48 mmol) in methanol (10 mL). After stirring the suspension for 30 min, the obtained dark blue solution was left to slowly evaporate to yield blue crystals. The crystals were recrystallized from a minimum amount of boiling methanol (38 mg, 23%).

UV-vis (MeOH, 5·10⁻⁶ M) [λ_{max}, nm (ε, mol⁻¹ cm²): 266 (33310), 362 (104300), 577 (3300). Anal. Calcd for C₁₁H₁₈CuN₄O₅·H₂O: C, 35.92; H, 5.48; N, 15.23; Found: C, 35.77; H, 5.09; N, 15.88.

[(L1)Cu][CF₃SO₃], 2. Analogous to **1**, from Cu(CF₃SO₃)₂ (174 mg, 0.48 mmol), 2-(2-(2-aminoethylamino)ethyl)iminomethylphenol (**L1H**) (100 mg, 0.48 mmol) in methanol (10 mL) stirred 30 min. The obtained blue solution was left to slowly evaporate to yield very few purple crystals, which were used without characterization other than X-ray studies.

[(L2)Cu][NO₃], 3. Analogous to **1**, from Cu(NO₃)₂·2.5 H₂O (85 mg, 0.36 mmol), 2-(2-(2-aminoethylamino)ethyl)iminomethyl-4,6-dichlorophenol (**L2H**) (100 mg, 0.36 mmol) in ethanol (10 mL) stirred 30 min to yield dark blue oil. The oil was crystallized from boiling ethanol (3 mL), to yield dark blue crystals which were then re-crystallized from a minimum amount of boiling ethanol (13 mg, 9%).

UV-vis (MeOH, 5·10⁻⁶ M) [λ_{max}, nm (ε, mol⁻¹ cm²): 267 (90000), 359 (25000), 570 (1000). Anal. Calcd for C₁₁H₁₄Cl₂CuN₄O₄·EtOH: C, 34.95; H, 4.51; N, 12.54; Found: C, 34.84; H, 3.95; N, 12.75.

[(L3)Cu][NO₃]₂·MeOH, 4. Analogous to **1**, from Cu(NO₃)₂·2.5 H₂O (100 mg, 0.43 mmol), 2-((2-(piperazin-1-yl)ethyl)iminomethyl)phenol (**L3H**) (100 mg, 0.43 mmol) in methanol (10 mL) stirred 30 min. The desired complex directly crystallized out of the dark green solution (65 mg, 33%).

UV-vis (MeOH, 7.5·10⁻⁶ M) [λ_{max}, nm (ε, mol⁻¹ cm²): 278 (76900), 300 (sh), 374 (22100), 632 (200). Anal. Calcd for C₁₃H₁₉CuN₅O₇·CH₃OH: C, 37.13; H, 5.12; N, 15.46; Found: C, 36.74; H, 5.01; N, 15.43.

[(L4)Cu(MeOH)][NO₃]₂·½MeOH, 5. Analogous to **1**, from Cu(NO₃)₂·2.5 H₂O (67 mg, 0.29 mmol), 2,4-di-tert-butyl-6-((2-(piperazin-1-yl)ethyl)iminomethyl)phenol (**L4H**) (100 mg, 0.29 mmol) in methanol (10 mL) refluxed 1 h to yield dark green crystals. The crystals were re-crystallized from a minimum amount of boiling methanol and washed with hexane (3 x 5 mL). (18 mg, 10%)

UV-vis (MeOH, $2.5 \cdot 10^{-6}$ M) [λ_{\max} , nm (ϵ , mol $^{-1}$ cm 2): 280 (173600), 316 (41400), 390 (45200), 632 (600). Anal. Calcd for C₂₂H₃₉CuN₅O₈ · ½ C₆H₁₄: C, 49.39; H, 7.50; N, 11.47; Found: C, 49.66; H, 7.12; N, 11.86. (Replacement of methanol by hexane assumed during drying and washing for EA.)

[(L5)Cu(OH₂)]AcO · H₂O, 6. Analogous to **1**, from Cu(OAc)₂ (78 mg, 0.43 mmol), 2-((2-(piperidin-1-yl)ethyl)iminomethyl)phenol (**L5H**) (100 mg, 0.43 mmol) in methanol (10 mL) stirred 30 min. The obtained green solution was left to slowly evaporate to yield green crystals. The crystals were recrystallized from a minimum amount of boiling methanol. (36 mg, 23%)

UV-vis (MeOH, $7.5 \cdot 10^{-6}$ M) [λ_{\max} , nm (ϵ , mol $^{-1}$ cm 2): 272 (81400), 306 (sh), 378 (22000). Anal. Calcd for C₁₆H₂₄CuN₂O₄ · H₂O: C, 47.11; H, 6.92; N, 6.87; Found: C, 47.59; H, 6.71; N, 6.68.

rac-Lactide polymerization. In a glove box, the desired amount of *rac*-lactide was placed into a pressure tube together with the catalyst. If required, a highly concentrated stock solution of an additive (BnOH, etc.) in toluene was added. The pressure tubes were then placed in a preheated oil bath at 140 °C. In kinetic experiments, samples were taken at specific time intervals, dissolved in CDCl₃, filtered through a short silica plug to remove copper catalyst, which was rinsed with additional CDCl₃, and studied by ¹H NMR. After drying, polymers were stored at –80 °C for further analysis.

Conversion was determined from ¹H NMR by comparison to remaining lactide. *P_r* values were determined from homodecoupled ¹H NMR spectra and calculated from $P_r = 2 \cdot I_1 / (I_1 + I_2)$, with *I*₁ = 5.20 – 5.25 ppm (*rmr*, *mmr/rmm*), *I*₂ = 5.13 – 5.20 ppm (*mmr/rmm*, *mmm*, *mrmm*). The integration of the left multiplet and right multiplet (*I*₁ and *I*₂) required only one, very reproducible dividing point of the integration, which was always taken as the minimum between the two multiplets. Nevertheless, *P_r* values showed a much higher variability than typically observed in these polymerizations. Investigations indicated incomplete removal of Cu(II) as the source of the high variations. Molecular weight analyses were performed on a Waters 1525 gel permeation chromatograph equipped with three Phenomenex columns and a refractive index detector at 35 °C. THF was used as the eluent at a flow rate of 1.0 mL min⁻¹ and polystyrene standards (Sigma–Aldrich, 1.5 mg mL⁻¹, prepared and filtered (0.2 mm) directly prior to injection) were used for calibration. Obtained molecular weights were corrected by a Mark-Houwink factor of 0.58.⁸⁰

X-ray diffraction studies. Crystal for X-ray diffraction were obtained from synthesis as described above. Diffraction data were collected on a Bruker Venture METALJET diffractometer (Ga K α radiation) or a Bruker APEX II microsource (Cu K α radiation).⁸¹ Data reduction was performed with SAINT,⁸² absorption corrections with SADABS.⁸³ Structures were solved by dual-space

refinement (SHELXT).⁸⁴ All non-hydrogen atoms were refined anisotropic using full-matrix least-squares on F^2 and hydrogen atoms refined with fixed isotropic U using a riding model (SHELXL97).⁸⁵ Further experimental details can be found in Table 3 and the supporting information (CIF). All crystals but **1** and **4** were weakly diffracting and yielded poor structural data. Structures should be considered as proof of connectivity mainly.

Acknowledgements

Funding was supplied by the NSERC discovery program (RGPIN-2016-04953) and the Centre for Green Chemistry and Catalysis (FQRNT). We thank Francine Bélanger for support with X-ray diffraction, Elena Nadezhina for elemental analysis, Marie-Christine Tang and Dr. Alexandra Furtos for MALDI analyses, and Dr. Antoine Douchez for support with 2D NMR. J. L. Jimenez Santiago contributed during his MITACS internship to ligand synthesis.

Supporting Information

Additional graphics and details of all polymerizations. Details of the crystal structure determinations (CIF). CCDC 1852773-1852778 contains the supplementary crystallographic data for this paper. The data can be obtained free of charge from The Cambridge Crystallographic Data Centre via www.ccdc.cam.ac.uk/structures.

References

- (1) Nagarajan, V.; Mohanty, A. K.; Misra, M. *ACS Sustainable Chem. Eng.* **2016**, *4*, 2899-2916.
- (2) Castro-Aguirre, E.; Iñiguez-Franco, F.; Samsudin, H.; Fang, X.; Auras, R. *Adv. Drug Delivery Rev.* **2016**, *107*, 333-366.
- (3) Slomkowski, S.; Penczek, S.; Duda, A. *Polym. Adv. Technol.* **2014**, *25*, 436-447.
- (4) Singhvi, M.; Gokhale, D. *RSC Adv.* **2013**, *3*, 13558-13568.
- (5) Hottle, T. A.; Bilec, M. M.; Landis, A. E. *Polym. Degrad. Stab.* **2013**, *98*, 1898-1907.
- (6) Inkinen, S.; Hakkarainen, M.; Albertsson, A.-C.; Södergård, A. *Biomacromolecules* **2011**, *12*, 523-532.

- (7) Ahmed, J.; Varshney, S. K. *Int. J. Food Prop.* **2011**, *14*, 37-58.
- (8) Paul, S.; Zhu, Y.; Romain, C.; Brooks, R.; Saini, P. K.; Williams, C. K. *Chem. Commun. (Cambridge, U. K.)* **2015**, *51*, 6459-6479.
- (9) MacDonald, J. P.; Shaver, M. P. In *Green Polymer Chemistry: Biobased Materials and Biocatalysis*, American Chemical Society: 2015; Vol. 1192, pp 147-167.
- (10) Guillaume, S. M.; Kirillov, E.; Sarazin, Y.; Carpentier, J.-F. *Chem.-Eur. J.* **2015**, *21*, 7988-8003.
- (11) Sauer, A.; Kapelski, A.; Fliedel, C.; Dagonne, S.; Kol, M.; Okuda, J. *Dalton Trans.* **2013**, *42*, 9007-9023.
- (12) Jianming, R.; Anguo, X.; Hongwei, W.; Hailin, Y. *Des. Monomers Polym.* **2013**, *17*, 345-355.
- (13) Huang, B. H.; Dutta, S.; Lin, C. C. In *Comprehensive Inorganic Chemistry II (Second Edition)*, Poepelmeier, J. R., Ed. Elsevier: Amsterdam, 2013; Vol. pp 1217-1249.
- (14) Dagonne, S.; Normand, M.; Kirillov, E.; Carpentier, J.-F. *Coord. Chem. Rev.* **2013**, *257*, 1869-1886.
- (15) Dagonne, S.; Fliedel, C. In *Modern Organoaluminum Reagents: Preparation, Structure, Reactivity and Use*, Woodward, S.; Dagonne, S., Eds. Springer Berlin Heidelberg: Berlin, Heidelberg, 2013; Vol. pp 125-171.
- (16) Carpentier, J.-F.; Liu, B.; Sarazin, Y. In *Advances in Organometallic Chemistry and Catalysis*, John Wiley & Sons, Inc.: 2013; Vol. pp 359-378.
- (17) dos Santos Vieira, I.; Herres-Pawlis, S. *Eur. J. Inorg. Chem.* **2012**, *2012*, 765-774.
- (18) Wheaton, C. A.; Hayes, P. G. *Comments Inorg. Chem.* **2011**, *32*, 127-162.
- (19) Dutta, S.; Hung, W.-C.; Huang, B.-H.; Lin, C.-C. In *Synthetic Biodegradable Polymers*, Rieger, B.; Künkel, A.; Coates, G. W.; Reichardt, R.; Dinjus, E.; Zevaco, T. A., Eds. Springer-Verlag: Berlin, 2011; Vol. pp 219-284.
- (20) Dijkstra, P. J.; Du, H.; Feijen, J. *Polym. Chem.* **2011**, *2*, 520-527.
- (21) Dagonne, S.; Fliedel, C.; de Frémont, P. In *Encyclopedia of Inorganic and Bioinorganic Chemistry*, John Wiley & Sons, Ltd: 2011; Vol.
- (22) Buffet, J.-C.; Okuda, J. *Polym. Chem.* **2011**, *2*, 2758-2763.
- (23) Thomas, C. M. *Chem. Soc. Rev.* **2010**, *39*, 165.
- (24) Sutar, A. K.; Maharana, T.; Dutta, S.; Chen, C.-T.; Lin, C.-C. *Chem. Soc. Rev.* **2010**, *39*, 1724-1746.
- (25) Stanford, M. J.; Dove, A. P. *Chem. Soc. Rev.* **2010**, *39*, 486-494.
- (26) Kiesewetter, M. K.; Shin, E. J.; Hedrick, J. L.; Waymouth, R. M. *Macromolecules* **2010**, *43*, 2093-2107.
- (27) Jones, M. D. In *Heterogenized Homogeneous Catalysts for Fine Chemicals Production*, Barbaro, P.; Liguori, F., Eds. Springer Netherlands: 2010; Vol. 33, pp 385-412.
- (28) Ajellal, N.; Carpentier, J.-F.; Guillaume, C.; Guillaume, S. M.; Helou, M.; Poirier, V.; Sarazin, Y.; Trifonov, A. *Dalton Trans.* **2010**, *39*, 8363.
- (29) Wheaton, C. A.; Hayes, P. G.; Ireland, B. J. *Dalton Trans.* **2009**, 4832 - 4846.
- (30) Amgoune, A.; Thomas, C. M.; Carpentier, J.-F. *Pure Appl. Chem.* **2007**, *79*, 2013-2030.
- (31) Wu, J.; Yu, T.-L.; Chen, C.-T.; Lin, C.-C. *Coord. Chem. Rev.* **2006**, *250*, 602-626.
- (32) Dechy-Cabaret, O.; Martin-Vaca, B.; Bourissou, D. *Chem. Rev.* **2004**, *104*, 6147-6176.
- (33) O'Keefe, B. J.; Hillmyer, M. A.; Tolman, W. B. *J. Chem. Soc., Dalton Trans.* **2001**, 2215-2224.
- (34) Specklin, D.; Hild, F.; Chen, L.; Thévenin, L.; Munch, M.; Dumas, F.; Le Bideau, F.; Dagonne, S. *ChemCatChem* **2017**, *9*, 3041-3046.
- (35) Lapenta, R.; Buonerba, A.; De Nisi, A.; Monari, M.; Grassi, A.; Milione, S.; Capacchione, C. *Inorg. Chem.* **2017**, *56*, 3447-3458.
- (36) Cui, Y.; Chen, C.; Sun, Y.; Wu, J.; Pan, X. *Inorg. Chem. Front.* **2017**, *4*, 261-269.
- (37) Liu, B.; Roisnel, T.; Maron, L.; Carpentier, J.-F.; Sarazin, Y. *Chem.-Eur. J.* **2013**, *19*, 3986-3994.
- (38) Susperregui, N.; Delcroix, D.; Martin-Vaca, B.; Bourissou, D.; Maron, L. *J. Org. Chem.* **2010**, *75*, 6581-6587.

- (39) Zhang, J.; Xiong, J.; Sun, Y.; Tang, N.; Wu, J. *Macromolecules* **2014**, *47*, 7789-7796.
- (40) Dai, Z.; Sun, Y.; Xiong, J.; Pan, X.; Wu, J. *ACS Macro Lett.* **2015**, *4*, 556-560.
- (41) Xiong, J.; Zhang, J.; Sun, Y.; Dai, Z.; Pan, X.; Wu, J. *Inorg. Chem.* **2015**, *54*, 1737-1743.
- (42) Sun, Y.; Xiong, J.; Dai, Z.; Pan, X.; Tang, N.; Wu, J. *Inorg. Chem.* **2016**, *55*, 136-143.
- (43) Chen, C.; Cui, Y.; Mao, X.; Pan, X.; Wu, J. *Macromolecules* **2017**, *50*, 83-96.
- (44) Chen, C.; Jiang, J.; Mao, X.; Cong, Y.; Cui, Y.; Pan, X.; Wu, J. *Inorg. Chem.* **2018**, *57*, 3158-3168.
- (45) Spassky, N.; Wisniewski, M.; Pluta, C.; Le Borgne, A. *Macromol. Chem. Phys.* **1996**, *197*, 2627-2637.
- (46) Ovitt, T. M.; Coates, G. W. *J. Am. Chem. Soc.* **1999**, *121*, 4072-4073.
- (47) Radano, C. P.; Baker, G. L.; Smith, M. R. *J. Am. Chem. Soc.* **2000**, *122*, 1552-1553.
- (48) Chisholm, M. H.; Gallucci, J. C.; Zhen, H.; Huffman, J. C. *Inorg. Chem.* **2001**, *40*, 5051-5054.
- (49) Sun, J.; Shi, W.; Chen, D.; Liang, C. *J. Appl. Polym. Sci.* **2002**, *86*, 3312-3315.
- (50) John, A.; Katiyar, V.; Pang, K.; Shaikh, M. M.; Nanavati, H.; Ghosh, P. *Polyhedron* **2007**, *26*, 4033-4044.
- (51) Bhunora, S.; Mugo, J.; Bhaw-Luximon, A.; Mapolie, S.; Van Wyk, J.; Darkwa, J.; Nordlander, E. *Appl. Organomet. Chem.* **2011**, *25*, 133-145.
- (52) Li, C.-Y.; Hsu, S.-J.; Lin, C.-I.; Tsai, C.-Y.; Wang, J.-H.; Ko, B.-T.; Lin, C.-H.; Huang, H.-Y. *J. Polym. Sci., Part A: Polym. Chem.* **2013**, *51*, 3840-3849.
- (53) Routaray, A.; Nath, N.; Maharana, T.; Sutar, A. k. *J. Macromol. Sci., Part A: Pure Appl. Chem.* **2015**, *52*, 444-453.
- (54) Williams, C. K.; Breyfogle, L. E.; Choi, S. K.; Nam, W.; Young, V. G.; Hillmyer, M. A.; Tolman, W. B. *J. Am. Chem. Soc.* **2003**, *125*, 11350-11359.
- (55) Labourdette, G.; Lee, D. J.; Patrick, B. O.; Ezhova, M. B.; Mehrkhodavandi, P. *Organometallics* **2009**, *28*, 1309-1319.
- (56) Rosen, T.; Popowski, Y.; Goldberg, I.; Kol, M. *Chem.-Eur. J.* **2016**, *22*, 11533-11536.
- (57) Zhu, H. L.; Li, S. Y.; He, W. M.; Yu, K. B. Z. *Kristallogr. - New Cryst. Struct.* **2002**, *217*, 599.
- (58) Plyuta, N. I.; Rusanova, J. A.; Petrusenko, S. R.; Omelchenko, I. V. *Acta Crystallogr., Sect. E: Struct. Rep. Online* **2014**, *70*, m330-m331.
- (59) Dieng, M.; Barry, A. H.; Gaye, M.; Sall, A. S.; Perez-Lourido, P.; Valencia-Matarranz, L. *Acta Crystallogr., Sect. E: Struct. Rep. Online* **2011**, *67*, m830-m831.
- (60) Bhunia, A.; Manna, S.; Mistri, S.; Paul, A.; Manne, R. K.; Santra, M. K.; Bertolasi, V.; Chandra Manna, S. *RSC Adv.* **2015**, *5*, 67727-67737.
- (61) Liu, G. X.; Ren, X. M.; Xu, H.; Tang, C. Y.; Wu, G. H.; CunChen, Y. *Chin. Chem. Lett.* **2004**, *15*, 1105.
- (62) Cusmano Priolo, F.; Rotondo, E.; Rizzardi, G.; Bruno, G.; Bombieri, G. *Acta Crystallogr., Sect. C* **1983**, *39*, 550-552.
- (63) The typical explanation for this is a long induction period. However, kinetic fits using this presumption are incongruent, yielding widely varying, even negative induction periods. Neither do conversion-time plots show the inflection point typically present in first-order reactions with an induction period. I. e. the rate in the early stages of the reaction does not increase in the early stages of reaction.
- (64) Xu, R.-B.; Xu, X.-Y.; Wang, M.-Y.; Wang, D.-Q.; Yin, T.; Xu, G.-X.; Yang, X.-J.; Lu, L.-D.; Wang, X.; Lei, Y.-J. *J. Coord. Chem.* **2008**, *61*, 3306-3313.
- (65) Chakraborty, J. J. *Korean Chem. Soc.* **2011**, *55*, 199.
- (66) Maxim, C.; Tuna, F.; Madalan, A. M.; Avarvari, N.; Andruh, M. *Crystal Growth & Design* **2012**, *12*, 1654-1665.
- (67) Gurumoorthy, P.; Mahendiran, D.; Prabhu, D.; Arulvasu, C.; Rahiman, A. K. *RSC Adv.* **2014**, *4*, 42855-42872.
- (68) Pait, M.; Kundu, B.; Kundu, S. C.; Ray, D. *Inorg. Chim. Acta* **2014**, *418*, 30-41.

- (69) Maity, T.; Saha, D.; Bhunia, S.; Brandao, P.; Das, S.; Koner, S. *RSC Adv.* **2015**, *5*, 82179-82191.
- (70) Ishani, M.; Prateeti, C.; Jaydeep, A.; Hulya, K.; Ennio, Z.; Antonio, B.; Antonio, F.; Debasis, D. *ChemistrySelect* **2016**, *1*, 615-625.
- (71) Mistri, S.; Paul, A.; Bhunia, A.; Manne, R. K.; Santra, M. K.; Puschmann, H.; Manna, S. C. *Polyhedron* **2016**, *104*, 63-72.
- (72) Kumari, S.; Mahato, A. K.; Maurya, A.; Singh, V. K.; Kesharwani, N.; Kachhap, P.; Koshevoy, I. O.; Haldar, C. *New J. Chem.* **2017**, *41*, 13625-13646.
- (73) Nesterova, O. V.; Nesterov, D. S.; Krogul-Sobczak, A.; Guedes da Silva, M. F. C.; Pombeiro, A. J. L. *J. Molec. Catal. A: Chem.* **2017**, *426*, 506-515.
- (74) Das, M.; Kumar Kundu, B.; Tiwari, R.; Mandal, P.; Nayak, D.; Ganguly, R.; Mukhopadhyay, S. *Inorg. Chim. Acta* **2018**, *469*, 111-122.
- (75) Whitehorne, T. J. J.; Schaper, F. *Chem. Commun. (Cambridge, U. K.)* **2012**, *48*, 10334-10336.
- (76) Whitehorne, T. J. J.; Schaper, F. *Inorg. Chem.* **2013**, *52*, 13612-13622.
- (77) Mondal, S.; Mandal, S. M.; Mondal, T. K.; Sinha, C. *Spectrochim. Acta, Part A* **2015**, *150*, 268-279.
- (78) Kilic, A.; Tegin, I.; Tas, E.; Ziyadanogullan, R. *J. Iran. Chem. Soc.* **2011**, *8*, 68-77.
- (79) Liu, R.-P.; Duan, M.-Y.; Li, J.; Su, Z.-P.; Zhang, J.-H.; Zhang, F.-X. *J. Struct. Chem.* **2011**, *52*, 935-940.
- (80) Save, M.; Schappacher, M.; Soum, A. *Macromol. Chem. Phys.* **2002**, *203*, 889-899.
- (81) Apex2, Release 2.1-0; Bruker AXS Inc.: Madison, USA, 2006.
- (82) Saint, Release 7.34A; Bruker AXS Inc.: Madison, USA, 2006.
- (83) Sheldrick, G. M. *Sadabs*, Bruker AXS Inc.: Madison, USA, 1996 & 2004.
- (84) Sheldrick, G. *Acta Crystallogr. Sect. A: Found. Crystallogr.* **2015**, *71*, 3-8.
- (85) Sheldrick, G. M. *Acta Crystallogr.* **2008**, *A64*, 112-122.

Figure 1. X-ray structures of **1** (left), **2** (middle) and **3** (right). Thermal ellipsoids are drawn at 50% probability. Hydrogen atoms other than those of water, non-coordinated anions, the second independent molecule for **3**, and the minor fraction of the disordered nitrate in **3** omitted for clarity.

Figure 2. Conversion-time plot for the polymerization of *rac*-lactide with **1**/benzyl alcohol at 140 °C. lactide:1:BnOH = 100:1:1. Black squares: single experiment with aliquots taken at desired times. Reaction was exposed to air during sampling. Blue diamonds: Series of 5 independent polymerization experiments quenched after 2, 4, 7 and 24 h. Reactions were not exposed to air. The inset shows the semi-logarithmic plot. Solid lines are theoretical conversions using the apparent first-order rate constant determined from the linear region of the semi-logarithmic plot

Figure 3. *rac*-Lactide polymerization with **1**/BnOH with different ratios of benzyl alcohol. Conditions: 140 °C, neat monomer, lactide:1 = 100:1, BnOH:1 = 1 (blue diamonds, 5 separate experiments), 1 (brown squares), 2 (black triangles), 4 (blue hollow diamonds), and 8 (red circles). The solid lines are theoretical conversions based on the pseudo-first-order rate constant determined from the linear region of the semilogarithmic plot (conversion < 70%). Left: Conversion-time plots, Upper Right: Semilogarithmic plots, Lower Right: Dependence of the observed pseudo-first-order rate constant on benzyl alcohol concentration.

Figure 4. Conversion-time plot for the polymerization of *rac*-lactide with **2** (blue diamonds). Data for **1** under identical conditions is provided for comparison (black squares). Conditions: 140 °C, lactide:[Cu]:BnOH = 100:1:1. The inset shows the semilogarithmic plot. Solid lines represent theoretical conversions based on the pseudo-first-order rate constant determined by linear regression of the semilogarithmic plots.

Figure 5. Conversion-time plot for the polymerization of *rac*-lactide with **1** in the presence of ammonium salts: 1 equiv [NEt₄]Cl (black triangle), 4 equiv [NEt₄]Cl (hollow triangle), 1 equiv [NEt₃H][TsO] (red circle), 4 equiv [NEt₃H][TsO] (hollow circle). Conditions: 140 °C, lactide:[Cu]:BnOH = 100:1:1. The inset shows the semilogarithmic plot. Solid lines represent theoretical conversions based on the pseudo-first-order rate constant determined by linear regression of the semilogarithmic plots for $t > 120$ min.

Figure 6. Conversion-time plot and the semilogarithmic plot for *rac*-lactide polymerizations with **3**. Conditions: lactide:**3**:BnOH = 100:1:1 (blue diamonds), 100:1:4 (red circles).

Figure 7. X-ray structures of **4-6**. Thermal ellipsoids drawn at 50% probability level. Hydrogen atoms, the second independent molecule in **5** and the anion disorder in **4** omitted for clarity.

Figure 8. Conversion-time plot and the semilogarithmic plot for *rac*-lactide polymerizations with **4**. Conditions: lactide:**4**:BnOH = 100:1:1. Hollow diamonds are independent reactions quenched after 0.5, 2, 4, and 7 h without exposing the reaction to air. In the remaining four experiments samples were taken in the desired intervals, exposing the reaction to air. Two reactions were conducted with twice (diamonds) or half (triangles) the total amount of reactants to verify the influence of external impurities.

Figure 9. Conversion-time plot and the semilogarithmic plot for *rac*-lactide polymerizations with **6**. Conditions: lactide:**6**:BnOH = 100:1:1 (squares, triangles), 100:1:4 (circles). Lines represent theoretical conversions calculated from the pseudo-first-order rate constants obtained from the linear regions of the semilogarithmic plot.

Draft

Table 1. Bond lengths in the X-ray structures of **1-6**

	1	2	3	4	5	6
Cu-O _{Phenol}	1.924(2)	1.906(6)	1.91(2)	1.921(3)	1.909(13)	1.923(11)
Cu-N(=C)	1.944(3)	1.939(7)	1.97(2)	1.931(4)	1.942(15)	1.920(13)
Cu-N' ^a	2.014(3)	1.995(8)	1.97(2)	2.079(4)	2.067(16)	2.094(14)
Cu-N'' ^a	2.011(3)	2.009(7)	2.03(2)			
Cu-X			2.50(1), 2.72(2)	1.998(3), 2.440(4), (2.618(4))	1.987(13), (2.769(14))	1.942(10), 2.275(11), (2.721(12))
Cu-OH ₂ /O(H)Me	2.320(2)	2.425(6)			2.352(13)	
τ	0.1	0.1		0.1	0.1	0.2

^a N' : first amino group. N'' : second amino group

Draft

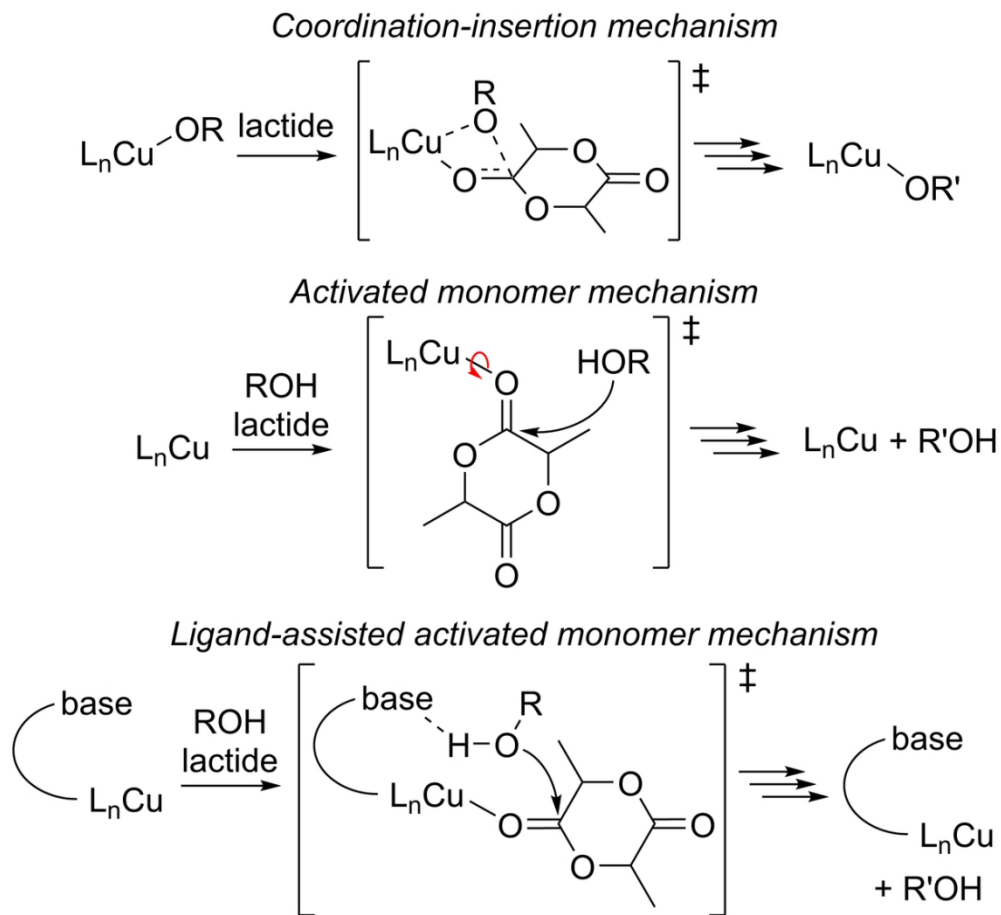
Table 2. Summary of *rac*-lactide polymerizations with 1-6/1 equiv benzyl alcohol ^a

Catalyst	LA:Cu:ROH ^b	Additive	Conversion ^c	k_{obs} [h ⁻¹] ^d	M_w/M_n ^e	#chains ^f	P_r ^g
1	100:1:1		94-96%	0.15(1)	2.9	17	0.65-0.85
1	100:1:1	5 H ₂ O	96%	0.37(1)	1.7	17	0.7-0.85
1	100:1:1	1-4 [NEt ₃ R]X	93-97%	0.37(1)-0.43(4)	1.6-1.8	9-18	0.6-0.85
2	100:1:1		95%	0.13(2)	1.5	9	0.8-0.85
3	100:1:1		95%	0.081(3), 0.26(4)	2.3	28	0.8-0.85
4	100:1:2 ^h		94-99%	0.16(1), 0.52(2)	1.3-1.4	12	0.6-0.75
4	50:1:2 ^h		97%	0.57(3)	1.7	12	0.85-0.9
4	200:1:2 ^h		94%	0.072(4), 0.15	1.1	>100	0.75-0.8
5	100:1:2 ^h		94-96%	0.10(1), 0.28(2)	1.5-2.0	15-27	0.8
6	100:1:1		95-96%	0.14(1), 0.34(4)	2.6-2.9	12-17	0.75-0.8

^a See Table S1 for all polymerization data. ^b LA = *rac*-lactide, ROH = total amount of alcohol present, i. e. co-crystallized alcohol + benzyl alcohol added. ^c Final conversion after overnight reaction. This value does not represent reactivity. ^d Determined by linear regression of the semi-logarithmic plot. Two values are provided if two linear regions were identified. In this case, the lower value always describes the rate at the beginning of the reaction. ^e Determined by GPC, see experimental section. ^f Number of polymer chains per Cu calculated from (conversion*[lactide]/[catalyst]* M_{lactide})/ M_n (GPC). ^g Determined from decoupled ¹H NMR, see experimental section. ^h Crystal structure contains co-crystallized methanol.

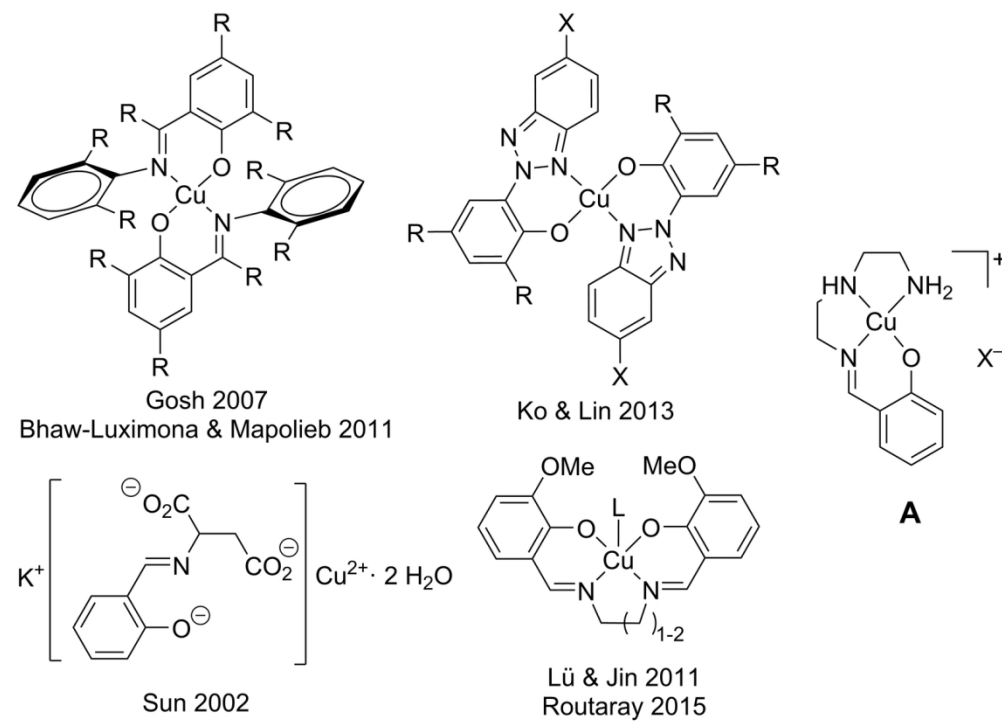
Table 3. Details of X-ray Diffraction Studies

	1	2	3	4	5	6
Formula	C ₁₁ H ₁₈ CuN ₄ O ₅	C ₁₂ H ₁₈ CuF ₃ N ₃ O ₅ S	C ₁₁ H ₁₄ Cl ₂ CuN ₄ O ₄	C ₁₄ H ₂₃ CuN ₅ O ₈	C ₄₅ H ₈₂ Cu ₂ N ₁₀ O ₁₇	C ₁₆ H ₂₄ CuN ₂ O ₄
M_w (g/mol)	349.83	436.89	400.70	452.91	1162.28	371.91
T (K); F(000)	150; 724	150; 1784	150; 812	150; 940	150; 2464	150; 1560
Crystal System	Monoclinic	Monoclinic	Triclinic	Monoclinic	Orthorhombic	Monoclinic
Space Group	$P2_1/c$	$P2_1/n$	$P\bar{1}$	$P2_1/n$	$Pna2_1$	$P2_1/c$
Unit Cell: a (Å)	9.1046(4)	20.6661(8)	7.1434(7)	9.5497(5)	20.8207(13)	9.7008(10)
b (Å)	14.6096(6)	7.2817(3)	10.8066(13)	14.8857(7)	8.3864(6)	18.6698(17)
c (Å)	10.8435(4)	24.2161(9)	19.909(2)	13.4561(6)	33.203(2)	23.501(3)
α (°)	90	90	96.025(8)	90	90	90
β (°)	102.117(2)	109.637(2)	90.517(8)	98.530(3)	90	101.775(7)
γ (°)	90	90	98.325(9)	90	90	90
V (Å ³); Z	1410.21(10); 4	3432.2(2); 8	1511.8(3); 4	1891.68(16); 4	5797.5(7); 4	4166.7(7); 8
μ (mm ⁻¹)	8.542	3.511	10.067	6.543	4.353	5.751
Absorption correction	multiscan	multiscan	multiscan	multiscan	multiscan	multiscan
θ range (°)	4.3-60.9	2.4-72	3.6-42.4	2.6-60.7	3.9-59.9	2.7-42.0
Completeness	1.0	1.0	0.96	1.0	0.98	0.99
Collected refl.; R_σ	17672; 0.0380	122587; 0.1259	7438; 0.1500	25277; 0.0670	45433; 0.1881	23048; 0.1223
Unique refl.; R_{int}	3198; 0.0567	72266; 0.1724	3106; 0.1205	4351; 0.0935	12938; 0.1750	4372; 0.1797
$R1(F)$ ($I > 2\sigma(I)$)	0.0530	0.1071	0.1648	0.0812	0.1461	0.1289
w $R(F^2)$ (all data)	0.1139	0.3005	0.4410	0.2140	0.4089	0.3823
GoF(F^2); Flack-x	1.15; -	1.04; -	1.04; -	1.04; -	1.13; 0.43(2)	1.20; -
Res. electron density	0.35; -0.45	2.81; -1.91	1.21; -0.67	0.72; -0.88	2.97; -0.76	0.92; -0.47



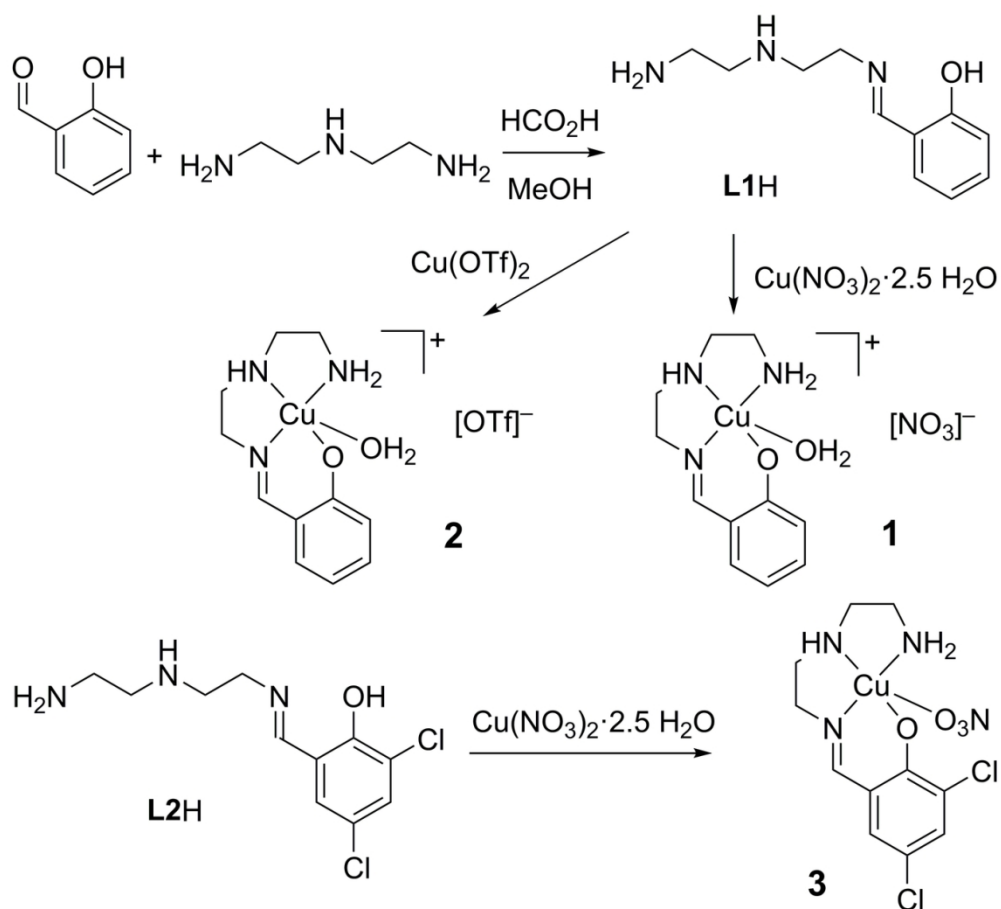
Scheme 1

105x97mm (300 x 300 DPI)



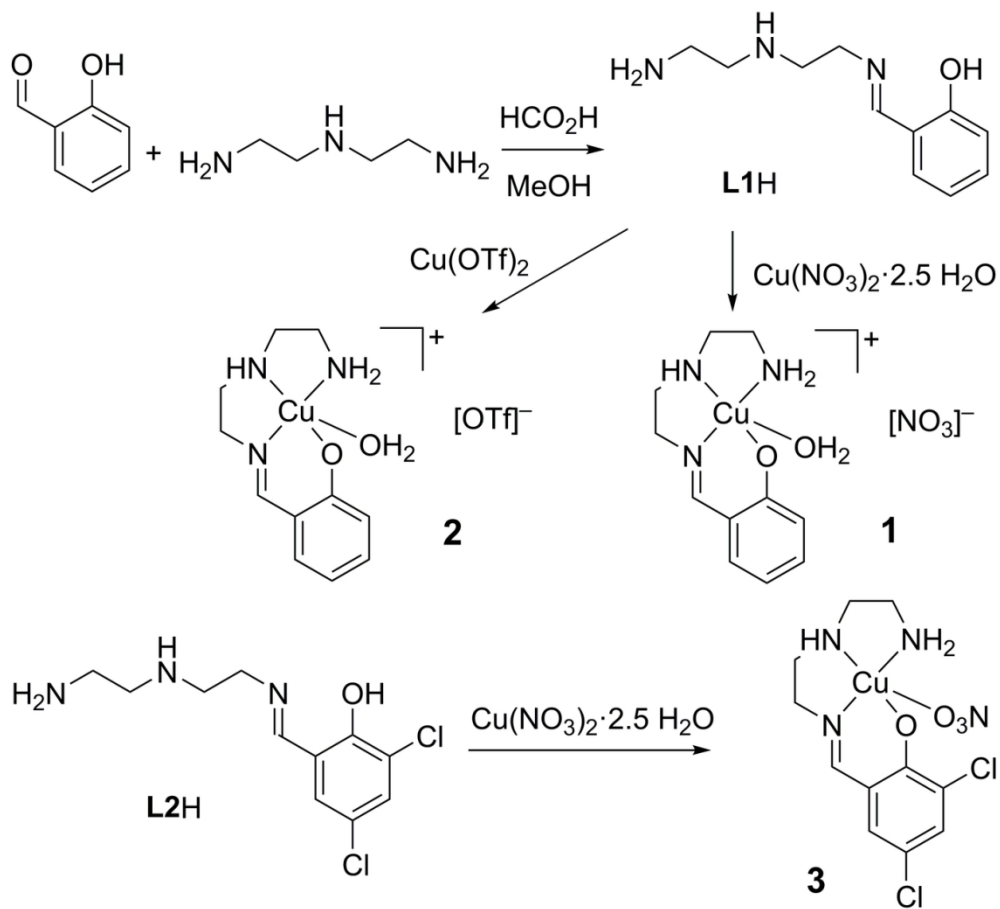
Scheme 2

140x101mm (300 x 300 DPI)



Scheme 3

118x108mm (300 x 300 DPI)



Scheme 4

118x108mm (300 x 300 DPI)

Figure 1

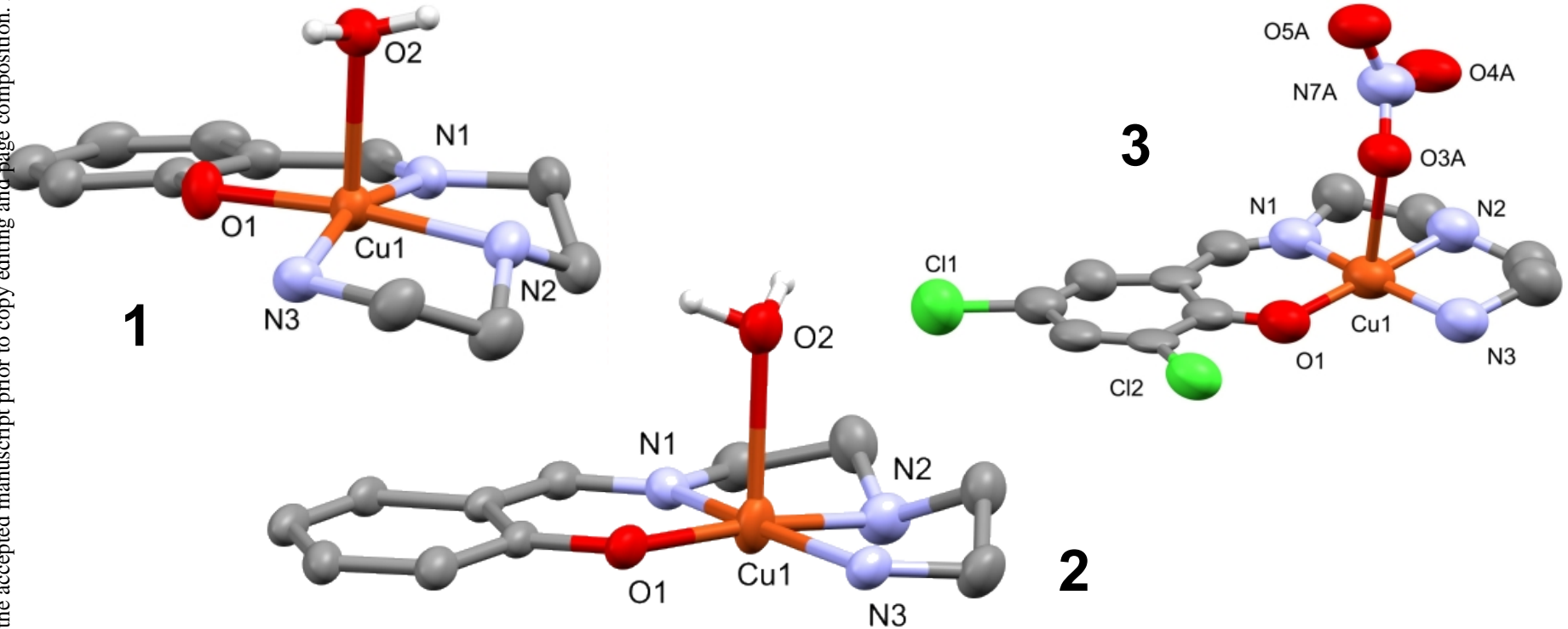


Figure 2

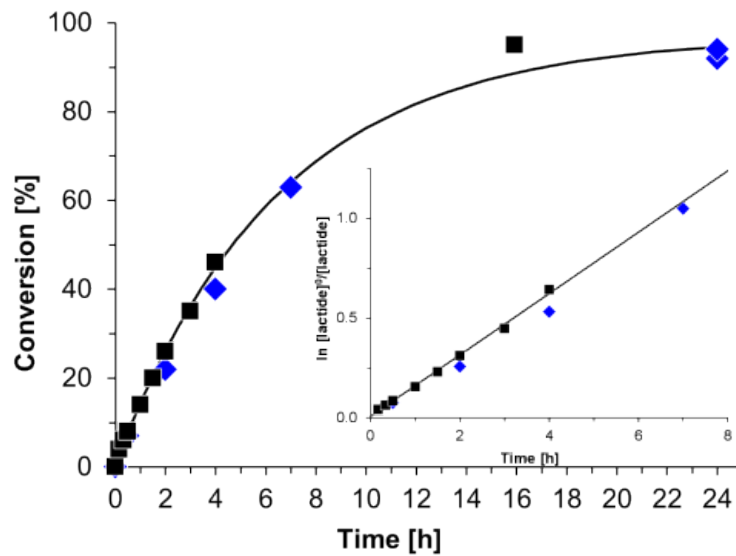


Figure 3

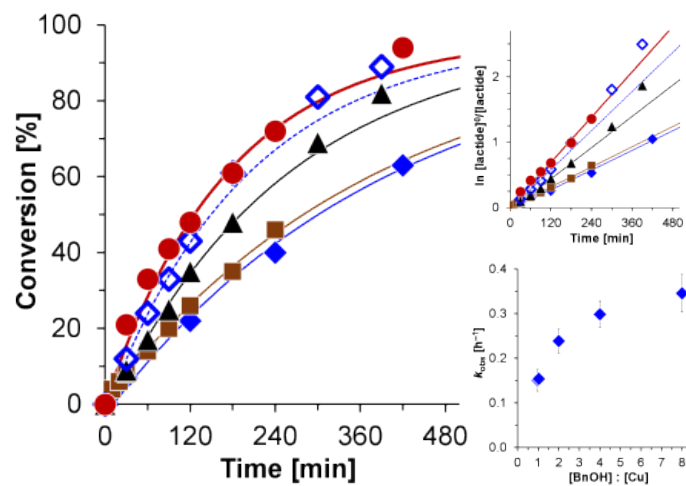


Figure 4

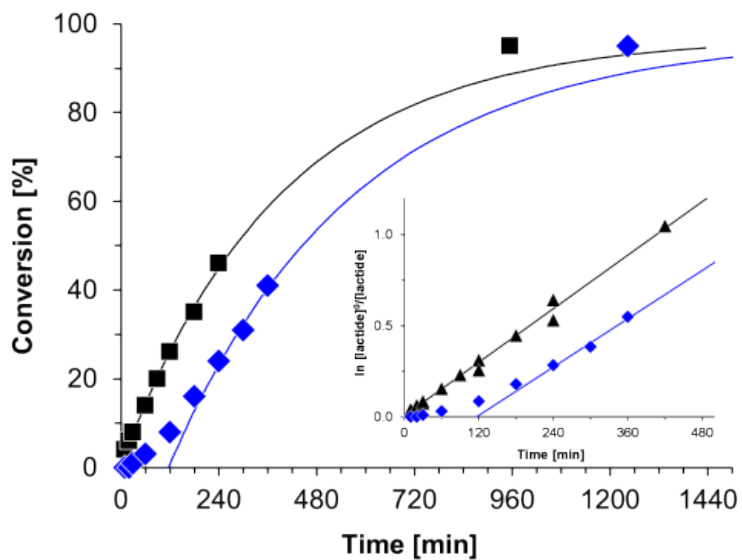


Figure 5

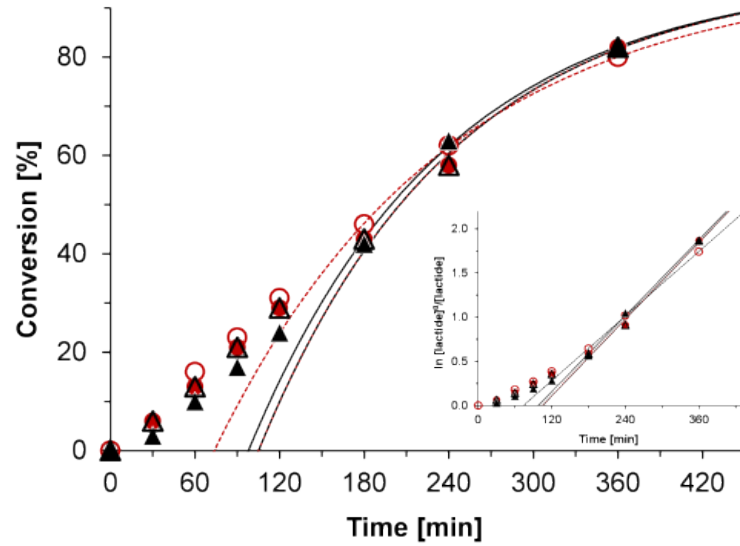


Figure 6

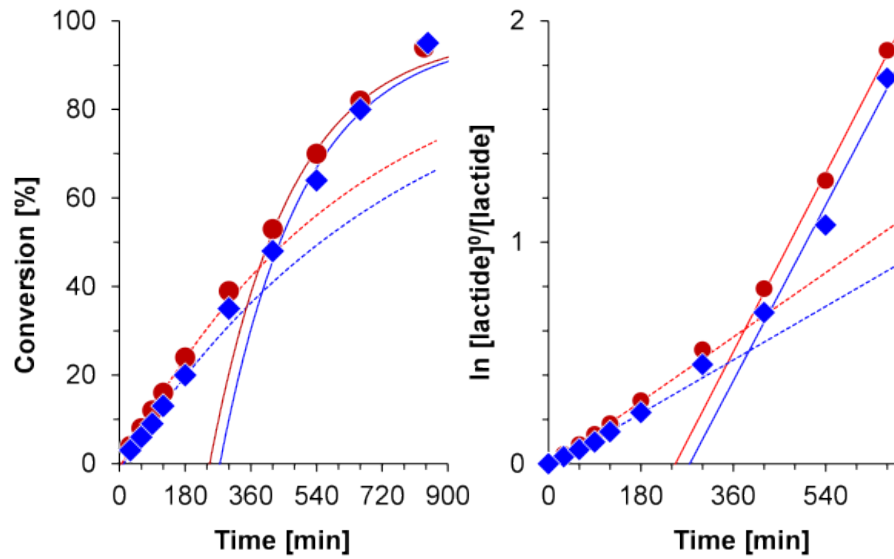


Figure 7

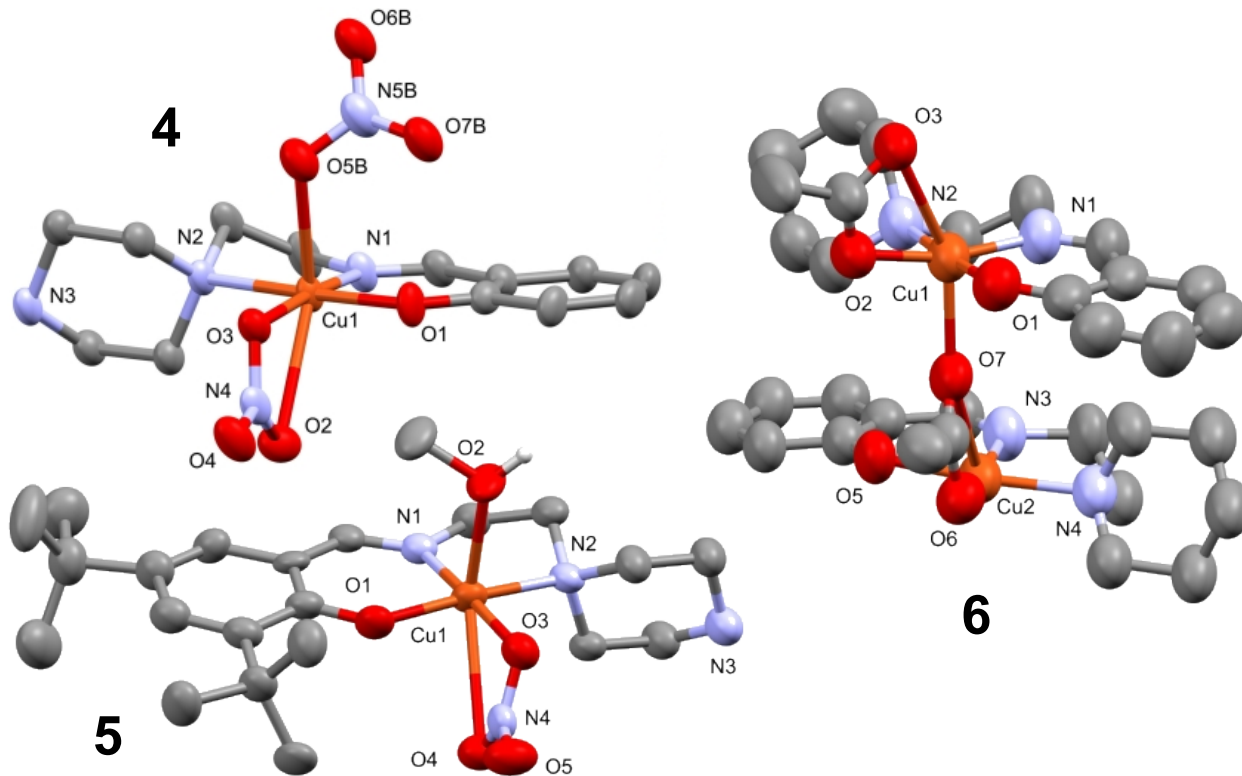


Figure 8

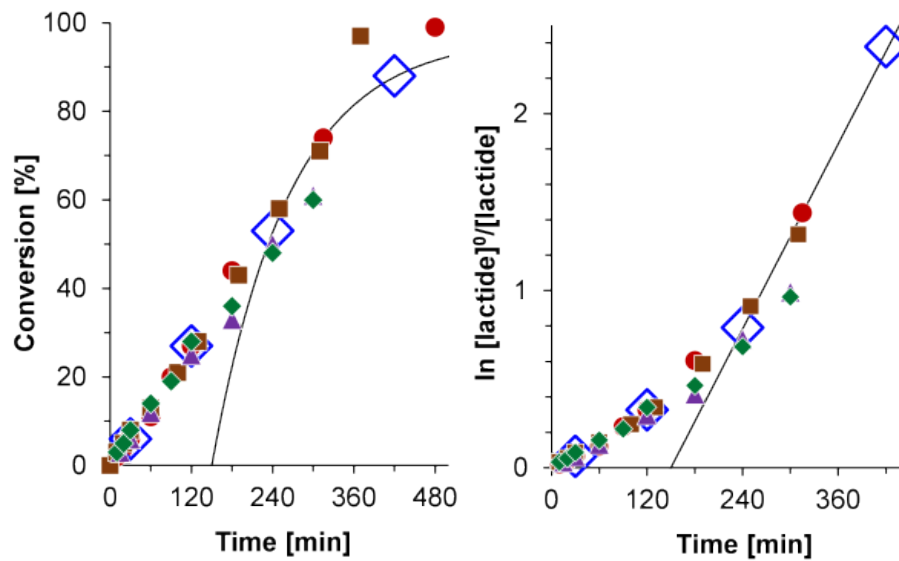
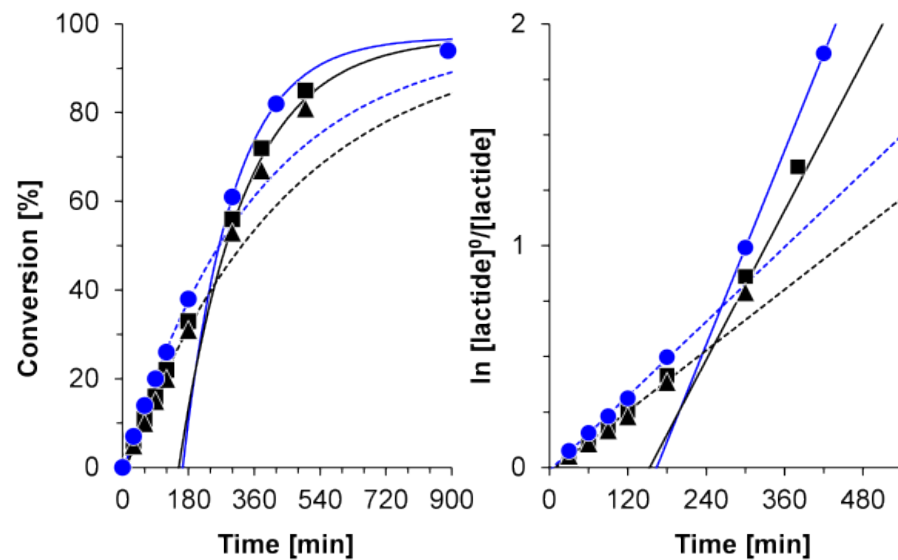


Figure 9



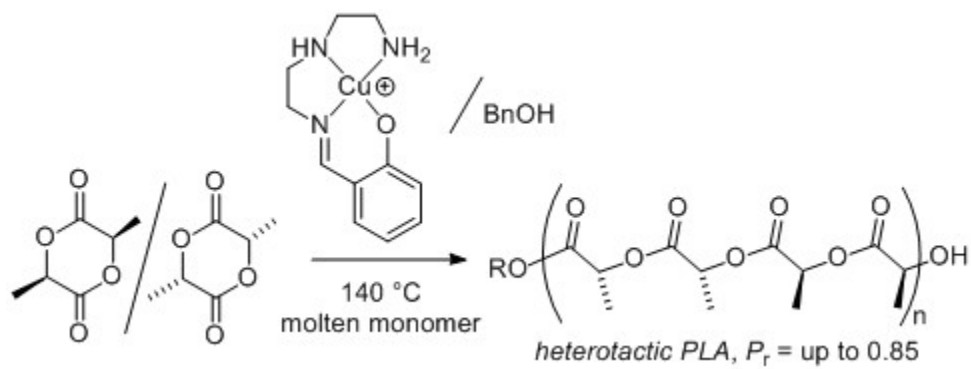


Table of contents graphics

128x48mm (96 x 96 DPI)